Geometrical analysis in material extrusion process with polylactic acid (PLA)+carbon fiber

Carolina Bermudo Gamboa
Ingeniería Civil, Materiales y Fabricación, Universidad de Málaga, Málaga, Spain, and
Sergio Martín Béjar, Francisco Javier Trujillo Vilches and Lorenzo Sevilla Hurtado
Department of Civil, Materials and Manufacturing Engineering, University of Malaga, Malaga, Spain

Abstract

Purpose – The purpose of this study is to cover the influence of selected printing parameters at a macro and micro-geometrical level, focusing on the dimensions, geometry and surface of printed parts with short carbon fibers reinforced PLA. For this case study, a hollow cylindrical shape is considered, aiming to cover the gap detected in previous works analyzed.

Design/methodology/approach – Nowadays, additive manufacturing plays a very important role in the manufacturing industry, as can be seen through its numerous research and applications that can be found. Within the engineering industry, geometrical tolerances are essential for the functionality of the parts and their assembly, but the variability in three-dimensional (3D) printing makes dimensional control a difficult task. Constant development in 3D printing allows, more and more, printed parts with controlled and narrowed geometrical deviations and tolerances. So, it is essential to continue narrowing the studies to achieve the optimal printed parts, optimizing the manufacturing process as well.

Findings – Results present the relation between the selected printing parameters and the resulting printed part, showing the main deviations and the eligible values to achieve a better tolerance control. Also, from these results obtained, we present a parametric model that relates the geometrical deviations considered in this study with the printing parameters. It can provide an overview of the piece before printing it and so, adjusting the printing parameters and reducing time and number of printings to achieve a good part.

Originality/value – The main contribution is the study of the geometry selected under a 3D printing process, which is important because it considers parts that are created to fit together and need to comply with the required tolerances. Also, we consider that the parametric model can be a suitable approach to selecting the optimal printing parameters before printing.

Keywords Additive manufacturing, Geometrical deviations, Roughness, PLA, Carbon fiber, Material extrusion processes, Tolerance

Paper type Research paper

1. Introduction

Additive manufacturing (AM) is becoming an interesting and extensively used technology in nowadays industry. It is constantly evolving, introducing new manufacturing ways, opening to new materials, like reinforced polymers, metals, ceramics, etc. and permitting the obtention of parts with great geometric complexity and shapes with low material waste, compared to conventional manufacturing processes like machining (Hanon and Zsidai, 2021; Hanon *et al.*, 2021).

AM processes were initially developed for rapid prototyping. However, thanks to the development of the technique, new printing processes are being developed (Singh *et al.*, 2018; Bedi *et al.*, 2020). Among the AM techniques, the material extrusion, Fused Filament Fabrication (FFF) or Fused Deposition Modeling (FDM) is one of the most used because of its simplicity, its economic advantage versus other manufacturing processes and its association with desktop three-dimensional (3D) printers, which open its usage to nonindustrial users, from commercial industry to educational use (Chacón *et al.*, 2017). FDM is based on the heating of a thermoplastic filament to a semiliquid state which make possible to deform it plastically and solidify fast in a new given shape. The material is deposited layer by layer until the 3D part

The current issue and full text archive of this journal is available on Emerald Insight at: **https://www.emerald.com/insight/1355-2546.htm**

Rapid Prototyping Journal
29/11 (2023) 21–39
Emerald Publishing Limited [ISSN 1355-2546]
[DOI 10.1108/RPJ-09-2022-0294]

Funding for open access charge: Universidad de Málaga/CBUA – Andalucia Tech Campus of International Excellence.

Author contributions: Conceptualization, CBG and SM.; methodology SM; data interpretation CBG and SM; writing – original draft preparation, CBG.; writing – review and editing, CBG, FJT, and SM; supervision, LS.; All authors have read and agreed to the published version of the manuscript.

Funding: This research received no external funding.

Conflicts of interest: The authors declare no conflict of interest.

Received 8 September 2022
Revised 11 November 2022
18 November 2022
Accepted 26 November 2022

is completed. Usually, the parts obtained by FDM do not require a demanding geometric control. Notwithstanding, the current technological development has allowed printing final pieces with controlled mechanical behavior, geometrical deviations and narrow tolerances (Sedighi *et al.*, 2020; Boğa and Seyedzavvar, 2021).

A great diversity of materials can be used for this process. Polylactic acid (PLA) and Acrylonitrile butadiene styrene (ABS) are used in general (Zhou *et al.*, 2018; Boğa, 2021), but their low mechanical properties has led to develop new materials with long or short fibers embedded like carbon fiber (CF), glass fiber (GF), carbon nanotubes, etc. (Yang *et al.*, 2017; Dizon *et al.*, 2018; Bilkar *et al.*, 2021). These new materials are turning the FDM concept, enabling it to produce final products conceived for mechanical applications and where geometric control is already a requirement for the validity of the product. Also, this technology is being implemented in different and new fields, like biology, medicine and engineering, with good results (Arbeiter *et al.*, 2018; Alam *et al.*, 2020). The materials most commonly used in the consulted literature to carry out tests and analyze the mechanical response of parts according to the printing parameters are ABS, reinforced ABS, PLA, reinforced PLA, nylon and polyethylene terephthalate glycol (PETG). PLA polymer is becoming an alternative to ABS because it is considered an environmentally friendly material, presents lower cost, can be reusable and has good mechanical properties (Bhagia *et al.*, 2021).

The reinforced polymers (polymer matrix composites) are becoming more interesting because of its improved performance versus unreinforced polymeric materials. The mechanical behavior of the parts can be improved adding fillers, fibers and particulate materials, resulting in composite material. This helps overcoming one of the big limitations on the use of FDM. However, the material processing becomes more complicated and delicate due to the reinforcement (Liu *et al.*, 2019; Arunkumar *et al.*, 2021). Short fiber filaments are preferable because can be implemented using the same printing techniques as for the unreinforced thermoplastics, even though continuous fiber gives better mechanical properties.

An optimization of the printing process is usually needed, having a broad range of parameters that can be analyzed: build speed, feed rate, temperature, build orientation and infill pattern, among others. The printing parameters affect not only the surface and visual effect of the printed part, but also are critical for the mechanical behavior of the samples. The parameters usually analyzed are the fill angle, layer thickness, filament width and printing orientation, among others. Lokesh *et al.* focus on the influence of the layer thickness, build orientation and raster angle on the mechanical properties of PLA specimens, conducting tensile strength tests, through Design of Experiment (DOE) by means of Taguchi and ANOVA (Lokesh *et al.*, 2021). The conclusions show that the layer thickness and the raster angle has negative correlation when combined with build orientation. The maximum UTS reached is at 45° build orientation, 0.1 mm layer thickness and 30° raster angle. Ahmed and Susmel focus solely on the deposition angle, from 0° to 90°, and its influence in the strength and fracture behavior of the parts, concluding that the fabrication direction, in this case study, has not significant influence (Ahmed and Susmel, 2017). Durga Prasada Rao *et al.* present the influence of layer thickness, print temperature and infill pattern on tensile strength of PLA+CF specimens, implementing ANOVA (Durga Prasada Rao *et al.*, 2019). The conclusions show that the maximum tensile strength is achieved with 0.1 mm layer thickness, 225°C extrusion temperature and a cubic structured infill pattern. Manav Doshi *et al.* present a review of printing parameters and its influence on the tensile strength, stress and Young's modulus, mainly focusing on the crucial printing parameters, that are considered to be the layer thickness, infill density and pattern, printing speed, build orientation and raster angle (Doshi *et al.*, 2022). They concluded that the 100% infill density offers the highest Young's modulus as well as the 0° raster angle. At 90 mm/s infill speed, the layer structure is the best, with the lowest porosity and hence, provided the best Young's modulus performance. Saifudding Khan *et al.* include in the analysis the flow rate, the speed, nozzle and air-gap formation in specimens considering different materials as ABS, PLA and polyethylene terephthalate (PET), among others (Khan *et al.*, 2022). They concluded that an increase in the layer thickness and printing speed leads to lower mechanical properties. Also, raster orientation has a significant effect on the mechanical properties, as well as the reinforcement in the material. The specimens tend to present better mechanical properties.

Even though diverse studies that work on the mechanical behavior of the printed parts can be found, as the ones mentioned above, there is a gap in the analysis of the geometric deviations of AM parts. Knowing that these geometrical deviations also affect the mechanical behavior of the obtained parts (Ahmed and Susmel, 2017; Durga Prasada Rao *et al.*, 2019; Doshi *et al.*, 2022) and that FDM printing equipment does not usually have a great capacity to manufacture large parts, so it is common to use components that are then destined to fit together, the study of the relationship of the printing parameters with the geometrical deviations of the samples is consider of interest. In addition, the part shape considered in this case study is a cylindrical tube, as a representation of parts printed to fit together (representing an axis and a hole). This can also be considered as a gap because the usual shapes analyzed are dog-bone, flat pieces or cylindrical without holes (Bilkar *et al.*, 2021; Srinidhi *et al.*, 2021; Khan *et al.*, 2022). Kovan *et al.* focus on a flat geometry based on the ASTM F2921 standard (Kovan *et al.*, 2017). It is concluded that the edgewise orientation (YZX) presents the highest adhesion strength with the lower thickness, whereas the flatwise (YXZ) samples present the opposite behavior. Allison *et al.* base the geometry on the ASTM D638 (Type 1) standard, the dog-bone shape (Allison *et al.*, 2016). They concluded that the maximum tensile and flexural strength is obtained with the lower thickness and lower printing speed (0.2 mm and 30 mm/s), due to a better bonding with previous printed layers. Similar shape is used by Raut *et al.* (2014), which shows that parts has good tensile strength and minimum cost for the *y*-axis at 0° built up orientation FDM. Ding *et al.* (2019) relate the printing parameters with the air pores occluded between layers. The less air pores, the better the mechanical results.

It can be seen that research on geometric properties in FDM AM is mostly focused on performance of unreinforced material, having the reinforced thermoplastic lesser analysis

extent (Spoerk *et al.*, 2020). Thus, more studies are essential to evaluate macro and micro-geometrical deviations.

This case study aims to analyze the influence of printing parameters mainly at a macro and micro-geometrical level, focusing on dimensional and geometrical deviations as well as surface quality with the roughness control. The parts are built with PLA+CF, because of the enhanced mechanical properties that the CF adds to the parts. Also, a hole cylindrical shape is considered to be able to analyze the influence of the printing process on axis and hole geometries. This study aims to cover the gaps detected in the literature consulted, presented in previous paragraphs. Also, based on the experimental results obtained, a parametric model that allows relating some of the analyzed geometrical deviation with the printing parameters studied is presented.

2. Materials and methods

In the present work, an experimental methodology has been followed for the manufacture and evaluation of the geometric deviations of the samples as the main objective, and the evaluation of the roughness and dimensional tolerance as complementary objectives.

2.1 Specimens manufacture

For the manufacture of the test specimens to be analyzed in this work, 1.75-mm PLA filament with CF (short fibers) has been chosen. PLA is one of the most used materials in 3D printing because of its ease of printing. It does not require a hot bed, requires low temperatures and is very little affected by warping. On the contrary, CF is a synthetic fiber with high stiffness, tensile strength and Young's modulus commonly used for reinforcing composite materials (Liao *et al.*, 2018; Yao *et al.*, 2018). As a result, the carbon reinforcement improves the mechanical properties of PLA, making it much more rigid at the cost of losing flexibility (Ferreira *et al.*, 2017; Arunkumar *et al.*, 2021). This also provides high structural strength. For the manufacture of the test specimens to be analyzed in this work, 1.75-mm PLA filament with CF (short fibers) has been chosen (i3D Tested brand). Thanks to the high percentage of PLA (85%) that the mixture contains, it benefits from its printability properties. In this case, the samples are not intended to be analyzed under any mechanical force. However, it is understood that PLA+CF is preferable for working-pieces manufacture, as they prove to present better mechanical behavior (Goh *et al.*, 2018; Suresha *et al.*, 2022).

Therefore, saving time and material is prioritized, as long as the execution of the different evaluation processes of the specimens are not affected. To be able to study the dimensional tolerance of the outer face, which would correspond to an axis, and the inner face, which would correspond to a hole, a shape of a hollow cylinder is selected (Figure 1). Also, being a single piece, speeds up the production of both printing and evaluation time and saves printing material. The dimensional conditions are stablished taking into account an average part that can be printed and that facilitate the measurement processes.

For this work, a total of 12 parameter combinations were considered, having a printed sample for each printing parameters combination. The IdeaMaker software has been used, which belongs to the Raise3D group of printers. During

Figure 1 Final sample dimensions

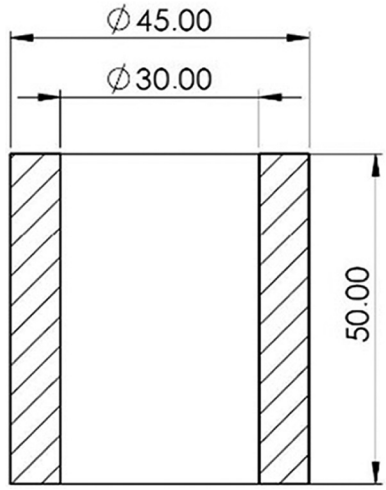

the lamination stage, the printing parameters have to be determined. In terms of filling, a filling density of 50% and a concentric pattern were chosen. Because the specimen is not intended to withstand stresses in this case study, the pattern that made the printing time shorter was chosen. For the solid fill, a linear pattern has been chosen, as it is the one that can be supported on the concentric fill pattern. The bed is heated at 60°C because, although PLA is an easy material to print even when the bed is not heated, if it is heated the chances of the part suffering warping decrease considerably.

As shown in Figure 2, the 3D printer "RAISE3D Pro2" was used for the production of the samples. This printer has double extruder, reaches a maximum of 300°C, a layer resolution down to 0.1 mm and working dimensions of 280 × 305 × 300 mm. As it is known, there are multiple printing parameters that could be adapted for an optimal printing process, presenting a complex analysis. So, it is necessary to narrow the selection, fixing printing parameters. For this case study, the parameters chosen for their influence analysis are the printing orientation, the layer thickness and the temperature. The rest of the variables are maintained constant.

So, to make an initial comparison of how printing orientation affects layer deposition, three horizontal and three vertical specimens, with a layer thickness of 0.3 mm, are printed. Table 1 shows the conditions for the printing process. The rest of the parameters have been maintained constant, as the nozzle size at 0.4 mm, the top and bottom solid layers as three layers with a 45° and 135° angle and three layers of perimeter shells.

It must be considered that the accuracy of the sample also depends on the flow rate (Culmone *et al.*, 2019; González-Henríquez *et al.*, 2019) which, in this case study, is maintained constant with no dimensional compensation of the part and a 100% filament flowrate set up with IdeaMaker.

As it can be seen, the printing speed considered is high compared to other general studies. This is because the study is intended to approximate the manufacturing time to the industry needs. The influence of the speed in the influence of the geometry of the part is studied aiming reducing this manufacturing time.

Figure 2 3D printer and software image

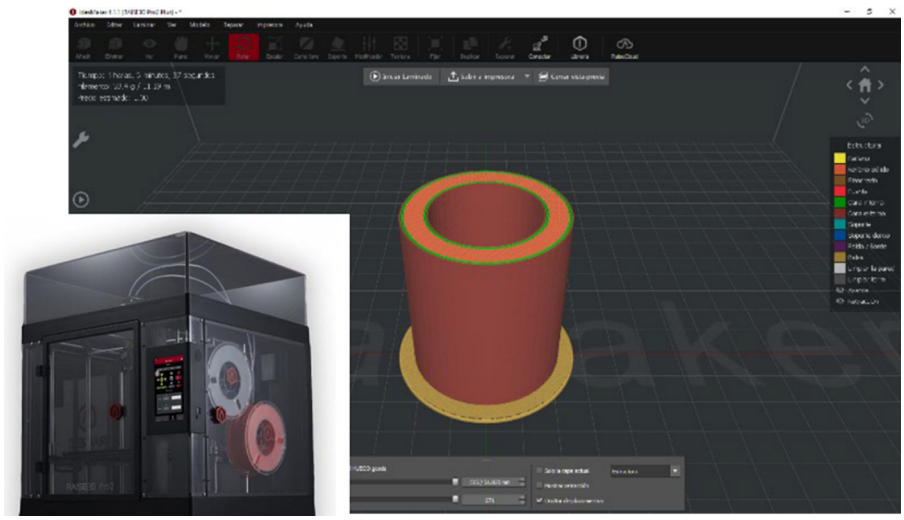

Table 1 Initial test conditions

Sample	Speed (mm/s)	Layer thickness (mm)	Temperature (°C)
Vertical	130	0.3	245
			230
			215
Horizontal	130	0.3	245
			230
			215

Figure 3(a) and 3(b) shows the software slicing with the 50% infill and the wall number of the printed specimens. The vertical specimens are printed with an initial three layers raft thicker than the layers of the samples. This facilitates the adherence. The slicing parameters that are not analyzed are maintained as constant. So, there are three shells considered, a 50% maximum shells overlap, extruder width 0.40 mm, retraction speed 40 mm/s, retraction material amount 0.50 mm and cooling enabled.

The raft is removed when the printing is finished [Figure 3(c)] to assure that the parts are measured as their finish stage, as they should work. The horizontal specimens were printed with and without support for a first comparation [Figure 3(d)]. The support improves the dimensional quality of the piece at the areas where the layers, because of the shape of the specimens, are supported in the air. For samples with overhanging features shallower than 45°, support is essential because new layers cannot be deposited onto thin air. However, it presents a detrimental

Figure 3 Slicing detail (a), 50% infill and walls number detail (b), vertical (c) and horizontal specimens specimens with and without support (d)

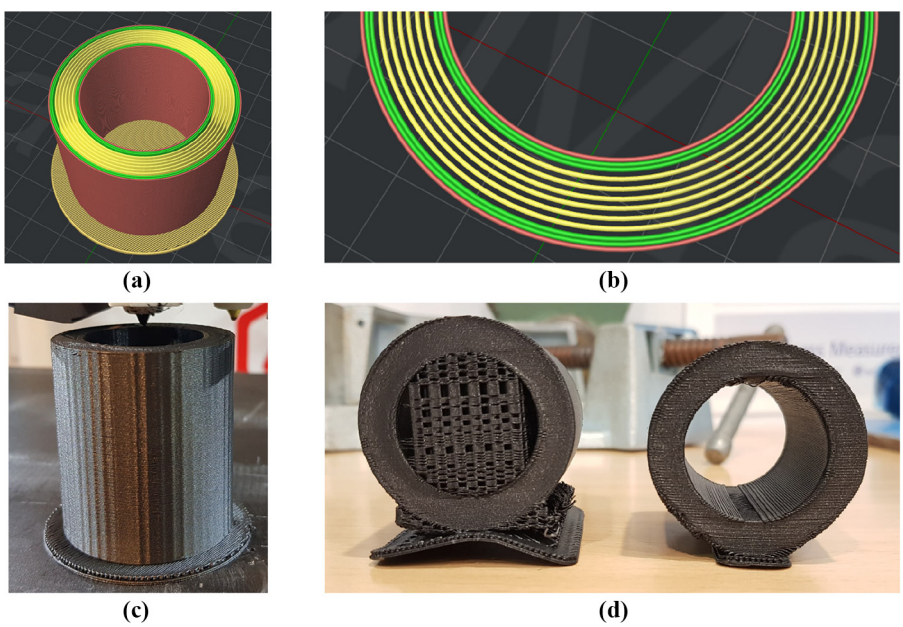

effect on the surface where the support is in contact with, presenting a rougher finish. For features less than 45°, it is possible to fulfil the printing process, with quality decrement depending on the angle (Redwood *et al.*, 2017).

Therefore, a pillar is made so that the layers are supported and the part does not deform. Notwithstanding, removing the support without damaging the specimen surface is difficult. The support for the outer face does not generate much damage but, the one on the inner face was difficult to remove completely and the inner surface has visible damage. For this reason, the horizontal specimens are printed without support, sacrificing precision. In addition, the fact of having a support or not can also result in an added experimental factor, so it is concluded that for the horizontal and vertical specimens are printed without support for equal printing conditions.

2.2 Dimensional control

Dimension deviations are controlled with a digital Vernier caliper (STANDARD GAGE, model V-DIGIT CAL 200 mm-8 in THUMB), E = 0.01 mm and a three-contact micrometer for interior measurements (MITUTOYO, model MAH2, range of use 25–30 mm), E = 0.01 mm.

First, the measurements of the inner diameter of the specimens are made. 16 measures are collected in total, corresponding to 4 measurements for each sample, each one at a different angle, at four different heights [Figure 4(a)].

The outer diameter is controlled in the same way with the digital Vernier caliper. 16 measures are obtained, corresponding to 4 measurements at different angles for each height [Figure 4(a)]. Also, the sample height, upper thickness and the lower thickness are controlled with the digital Vernier caliper, obtaining four data for each one. Each measurement has been made at 90° (*H1*, *H2*, *H3*, *H4*), starting always at the same vertical mark on the specimens, caused by the printing process, as is shown in Figure 4(b).

Figure 4 (a) Measurement positions and (b) deposition starting point for each layer during printing process

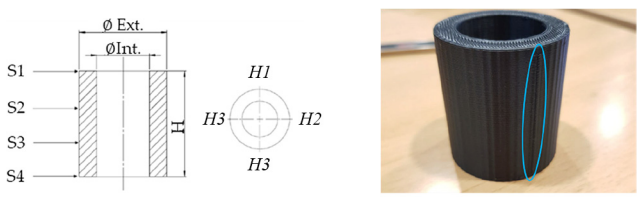

(a) (b)

2.3 Macro and micro-geometric deviations

For the roughness control, a roughness meter (MITUTOYO, model SURFTEST SJ-210) is used. The measurement length is stablished as l = 25 mm and 8 measurements were made inside and outside the samples, being a total of 16 measurements. For each one, the arithmetical mean roughness (*Ra*) and the maximum height of the roughness profile (*Rz*) are obtained. The order of measurement has been the same as stablished previously.

As for the macro-geometric deviations, the geometrical deviation measurement machine (ACCRETECH, model RONDCOM NEX) presents a sensitivity of 0.01 μm, being able to mark up to 14,000 measurement points. The specimens are fixed on the leveling bed using the raft on which it has been printed [Figure 5(a)] and the cero position is configured. In this case, the raft helps fixing and centering the printed part, having all the surface of the sample free for measurement, as it can be seen in Figure 5(a). After removing the raft, several measurements were carried out to assure that the action of removing the raft did not significantly alter the printed parts. The deviations obtained are of the same range because the ones obtained during the measurement with the raft and so, the raft is maintained to facilitate the measurement process.

With the aim of ensuring repeatability, several measurements were carried out along the specimen [Figure 5(b)]. Six different measurements are made from which 14 data groups are originated. The specimen is measured internal and externally. The roundness (RON) is expressed as the average result in these sections. Nine measurement points are taken on the Z axis, separated from each other by 5 mm, starting at point Z = 5 mm and ending at point Z = 45 mm. The straightness (STR) is controlled by 12 measurement points that are taken and gathered into 3 groups, depending on the position on the Z axis in which it is located. The measurements have a vertical length of 10 mm and the points Z = 5 mm, Z = 20 mm and Z = 35 mm are taken four times, separated from each other by 90°. From these data, the cylindricity (CYL) was calculated. As for the flatness (FLA), a single measurement point is taken, the inner edge of the upper face.

Among the different mathematical methods available for geometrical deviation analysis, the least squares circles method (Sui and Zhang, 2012) is applied for the roundness in this work. To evaluate the least square circumference center, a nonlinear iterative mathematical model is considered, minimizing the function error with the Sum of the Squared Errors equation [SSE; equation (1)] and taking the seed as the

Figure 5 (a) Sample fixation and (b) geometrical deviations controlled

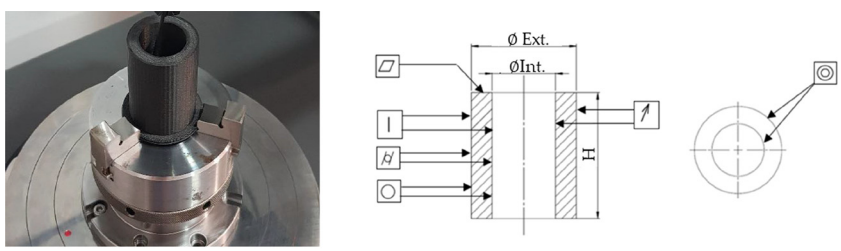

(a) (b)

rotation center. T SSE sum provides the system of equations that must be solved to get the fitting coefficients for the mathematical model to which one the data fit, obtaining the fitting coefficients that minimize the SSE.

$$SSE(a,b) = \sum_{i=1}^{n}\left(R - \sqrt{(x_i - a)^2 - (y_i - b)^2}\right) \quad (1)$$

where the different variables correspond with:

- R: radius of the profile;
- x_i: x coordinate of profile point;
- y_i: y coordinate of profile point;
- a: x coordinate of the center of the least square circumference; and
- b: y coordinate of the center of the least square circumference;

Then, RON is calculated as the difference between the radiuses of two concentric circumferences ($\mathcal{J}_{max} - \mathcal{J}_{min}$) which delimit the area containing all the points of the profile, as in Figure 6(c). The CON is the distance between the rotation center (0, 0) and the least squares circumference center previously obtained (a, b) [equation (2)].

$$CON = \sqrt{a^2 + b^2} \quad (2)$$

The straightness (STR) is calculated as the distance between two parallel lines ($D_{max} - D_{min}$) which delimit the area containing all the profile points and are parallel to the least square regression line [Figure 6(a)]. Finally, the cylindricity (CYL) is obtained as the difference between two co-axial cylinders, such that their radial difference is minimum ($P_{max} - P_{min}$), as in Figure 6(b).

3. Results and discussion

An initial study has been carried out to compare the results of the vertical specimens with a thickness of 0.3 mm with the horizontal ones of the same thickness, and the influence of the printing orientation is shown. On the contrary, the results of the vertical specimens have been compared, seeing the influence that the change in the extrusion temperature and layer thickness, considering the same printing orientation may has on the printed samples.

3.1 Horizontal versus vertical printing analysis

Controlling the dimensional deviations of FDM is not easy because of the nature of the process. When layers are deposited, the newly printed layer compresses and reheats the existing build layer, deforming its shape from round to oval and so, increasing the width of the extruded filament (Redwood, Schöffer and Garret, 2017). Also, because of the action of gravity, the plasticity of the deposited filament at printing temperature and the absence of support, horizontal specimens tend to collapse by its own weight. This may also explain the height increase, as when a cylinder is flattened, reducing its cross section, it elongates by the dimension of its axis.

Figure 7(a) represents the internal (30 mm) and external diameter (45 mm) mean deviation for the samples printed

Figure 6 Macrogeometrical deviations: (a) STR, (b) CYL and (c) RON and CON

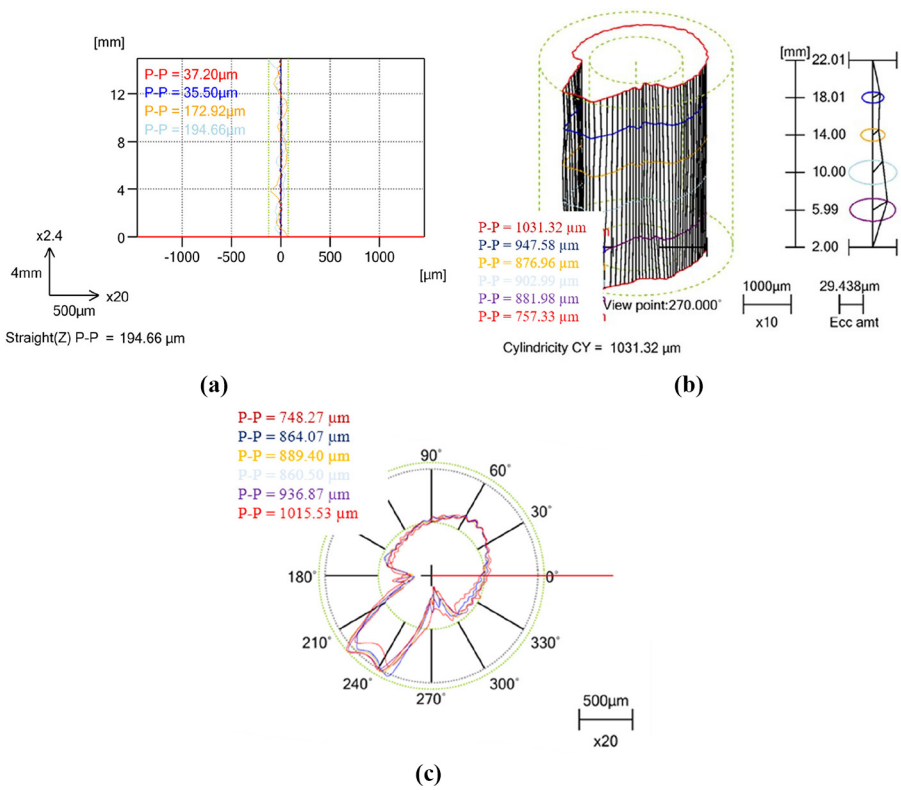

Figure 7 (a) Diameter and (b) height deviations for horizontal and vertical printed samples (%)

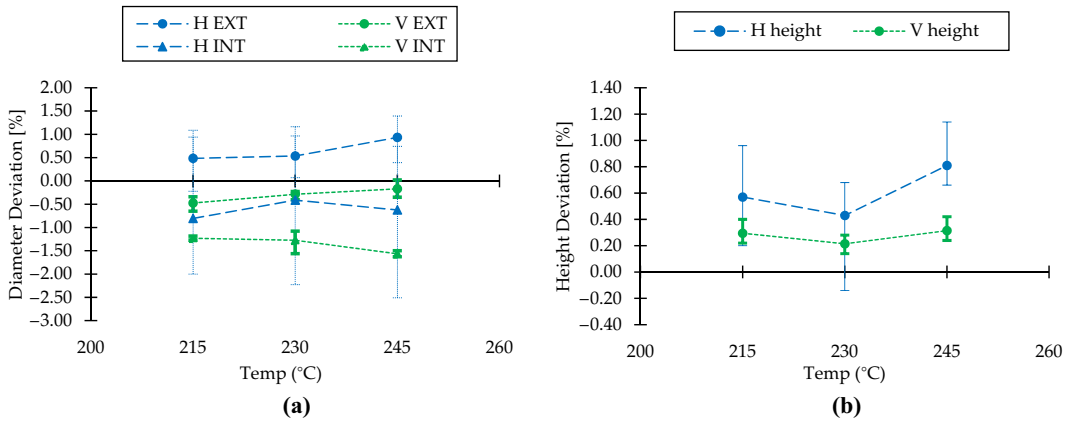

horizontally and vertically, at different temperatures, stablishing thickness at 0.3 mm. Although the own printer deviations have to be taken into account, it can be appreciated that, when printed horizontally, the samples present a greater deviation of the external diameter. Also, as the temperature increment, this deviation behaves in the same way, incrementing the diameter. This can be explained because when the temperature is higher, the plasticity of the material increases, the oval shape of the filament is more pronounced and so, the external diameter is affected. This effect can also be seen for the inner diameter, where, because of the oval shape of the filament, the inner diameter is smaller, although the shape and temperature effect is less evident for the horizontal sample than for the vertical one.

For the height deviations, it is clear that the horizontal printing position presents greater deviations. The weight of the layers in the vertical samples restrain the layers of expanding in the z-direction. As for the horizontal samples, the same weight of the layers and the compression of the nozzle tend to expand the shape. It can also be appreciated that the temperature affects more to the horizontal ones, because the material in a high plasticity state is free to flow in the x-direction. The difference in the behavior due to temperature can be set between 205°C and 245°C.

Also, it can be appreciated that the value dispersion is higher for the horizontal samples due to the printing process at that sample position.

In Figure 8, the macro-deviations for both horizontal and vertical samples are presented. It can be appreciated that the horizontal specimens show greater deviations in general. This tendency is normal because of the printing directions, that generated larger deformation for round shapes. As the filament behavior, the samples tend to be oval instead of round. This can be easily seen in Figure 8(a) and 8(b), where RON and Cylindricity (CYL) show deviations between 15 and 25 μm for horizontal samples, compared to 3 to 5 μm of the vertical ones. Because the round shape is compromised for the horizontal parts, the concentricity (CON) and the coaxiality (COX) also show greater deviations than the vertical parts [Figure 8(c) and 8(d)], being the vertical deviations close to 0. As for the STR, both printing directions present similar deviations, being the horizontal ones the parts with worst behavior in general.

So, after this first analysis, it can be concluded that the vertical printing direction present better results and so, the study is continued with the vertical configuration, as seen in Table 2.

3.2 Dimensional analysis

The results shown in these figures and the figures of the following sections are obtained from the vertical samples. For the outer diameter, Figure 9(a) and 9(b) represents its variations according to the temperature and the layer thickness. It can be appreciated that the greater the layer thickness, the closer to the nominal value is the diameter measured. This can be explained because of the plasticity of the material and its contraction when cooling. Having more material in the layer thickness, the more pronounced is the oval shape and so, this deformation of the filament improves the approximation of the external diameter to the nominal value. Also, having more material, the deposited filament needs more time for cooling and so, the contractions of the material are less marked. This can also be appreciated in Figure 9(b), where it can be seen that the influence of the temperature is not of great value but, when the material is printed at the higher temperature considered, it also needs more time for cooling and so the layer can be more deformed by the weight of the upper ones and the contractions do not reverse much the oval deformation, having a closer external diameter to the nominal one.

As for the interior diameter [Figure 9(c)], again, the oval deformation when the greater layer thickness is printed is high resulting in a smaller interior diameter and so, E = 0.3 mm present a higher deviation from the nominal value. The same behavior as expressed before for Figure 9(b) can be seen in Figure 9(d), where the temperature is not of great influence but, at the higher one, the material has more time for cooling and so, it has a greater deviation from the nominal value.

For the thickness of the part, the measurement is done on the upper [free, Figure 9(e) and 9(f)] and down [in contact with the hot bed, Figure 9(g) and 9(h)] part of the samples.

Figure 8 (a) Roundness, (b) cylindricity, (c) concentricity, (d) coaxiality and (e) straightness deviations for horizontal and vertical printed samples (μm)

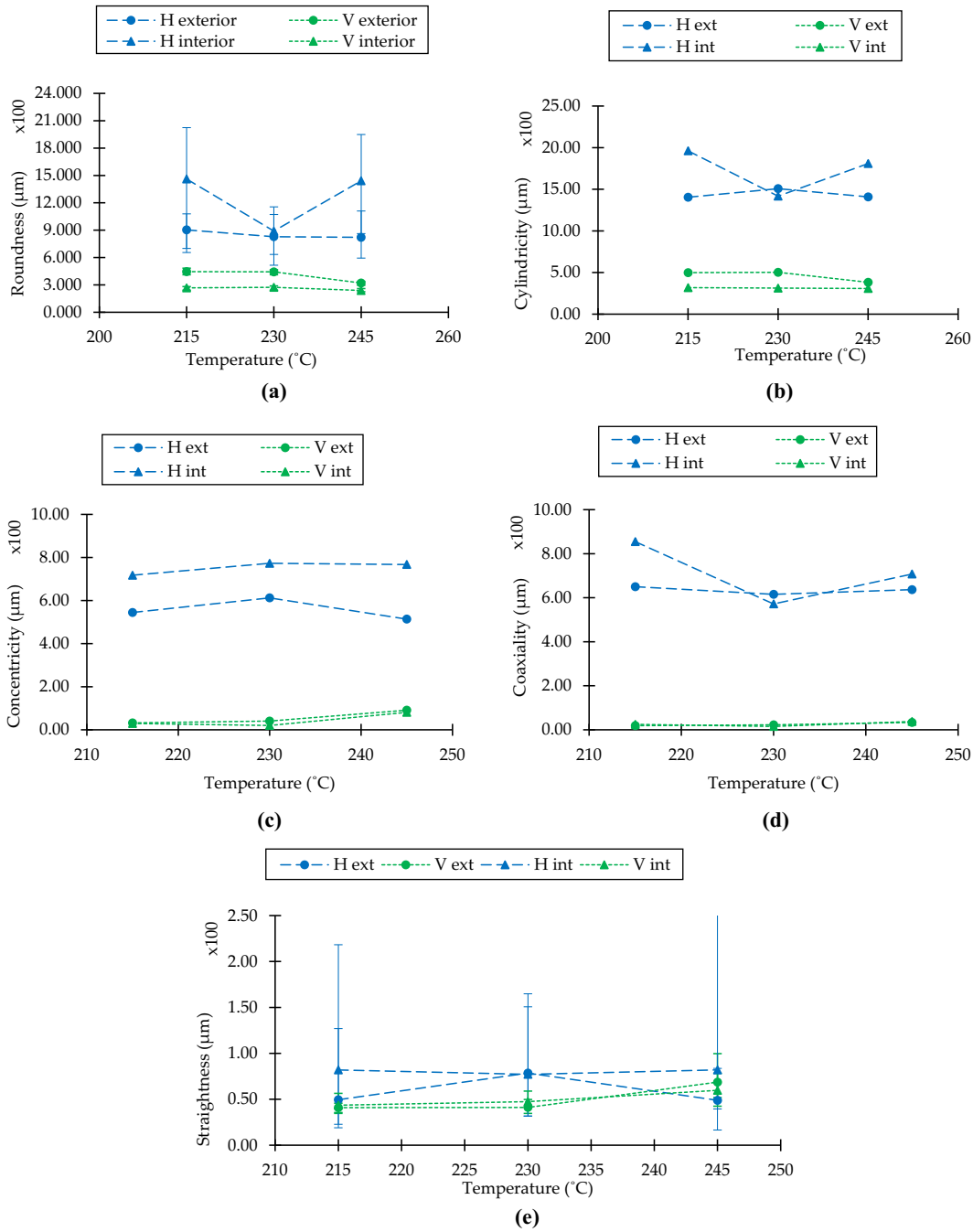

Table 2 Initial test conditions

Sample	Speed (mm/s)	Layer thickness (mm)	Temperature (°C)
Vertical	130	0.3	245
			230
			215
		0.2	245
			230
			215
		0.1	245
			230
			215

It can be seen that the upper part presents more deviation and both the temperature and the layer thickness have a representative influence. This can be explained because of the contact with the hot bed and the weight of the layers. The upper part has more freedom because it is not that much restrained with the weight and heat of the layers deposited over the printed ones and the also heat is not maintained with the temperature of the hot bed. The down part requires more time to cool than the upper part, because of the maintenance of the temperature and so, the material has more time to expand on the horizontal plane.

This is due to the printing process itself. The deposited filament remains plasticized, and as layers are added to the top, the weight supported by those at the base increases, which tend to crush and suffer a consequent increase in its surface. In addition, in the lower part, the specimen is supported by a raft, which hinders the possible volumetric contraction when it cools. That is why a higher deviation from the nominal value can be appreciated for the down thickness.

For the height of the samples, even though the oval shape can be more pronounced with thicker filaments and higher temperatures, the vertical plane is also incremented because of the increase in the material thickness, which can be seen in Figure 9(i) and 9(j). The deformation presented in the samples due to the contractions and plasticity of the material is not enough to compensate the growth in the z-axis. The temperature influence can be better appreciated for the 0.1 and 0.2 mm filaments [Figure 9(i)]. This can be explained because, the higher the temperature, the more time the sample needs to stabilize with the exterior temperature and the contractions are less pronounced.

Figure 9 (a) Exterior diameter, (b) interior diameter, (c) superior and (d) inferior thickness and (e) height deviations for vertical printed samples (%)

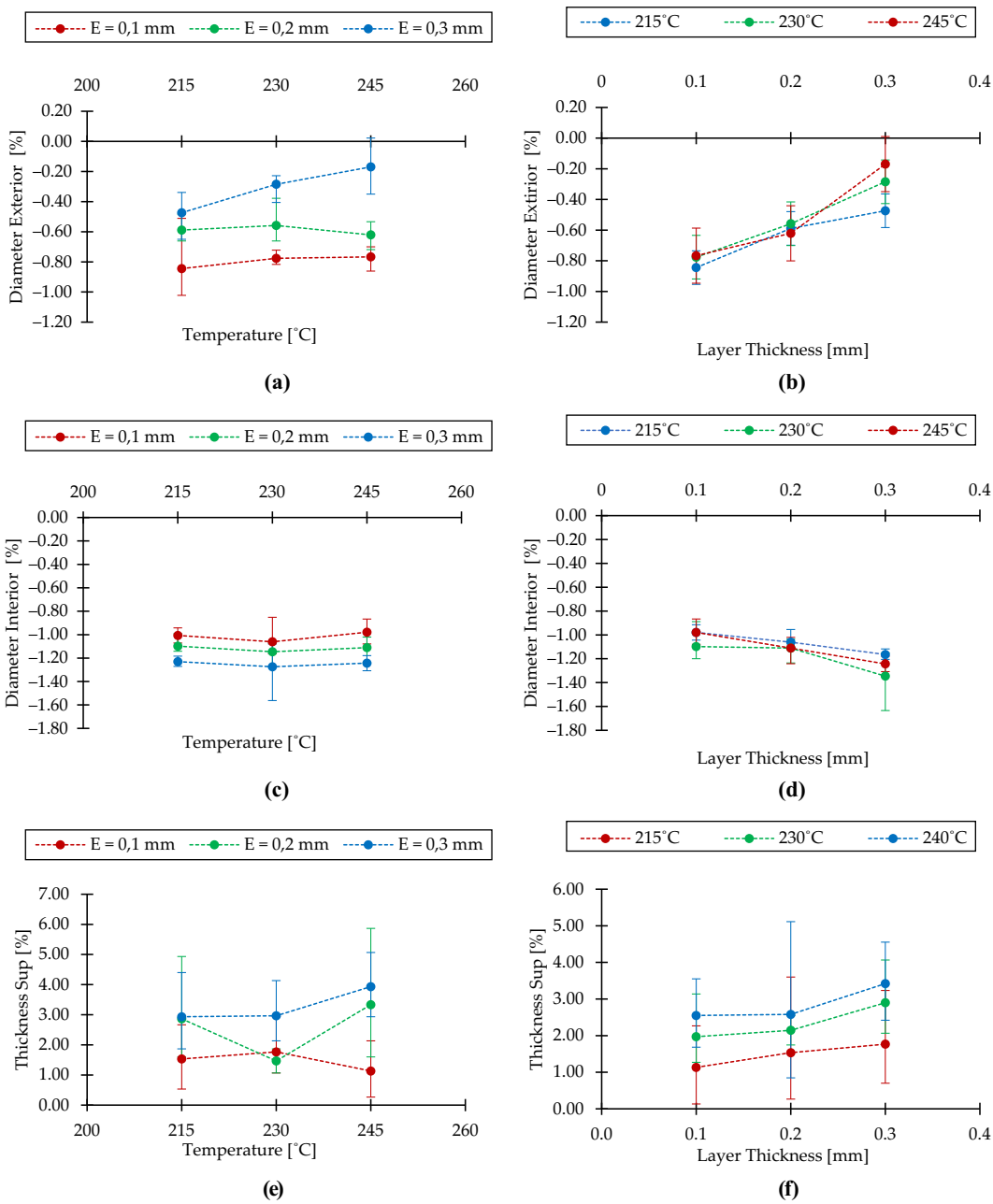

(*continued*)

Figure 9

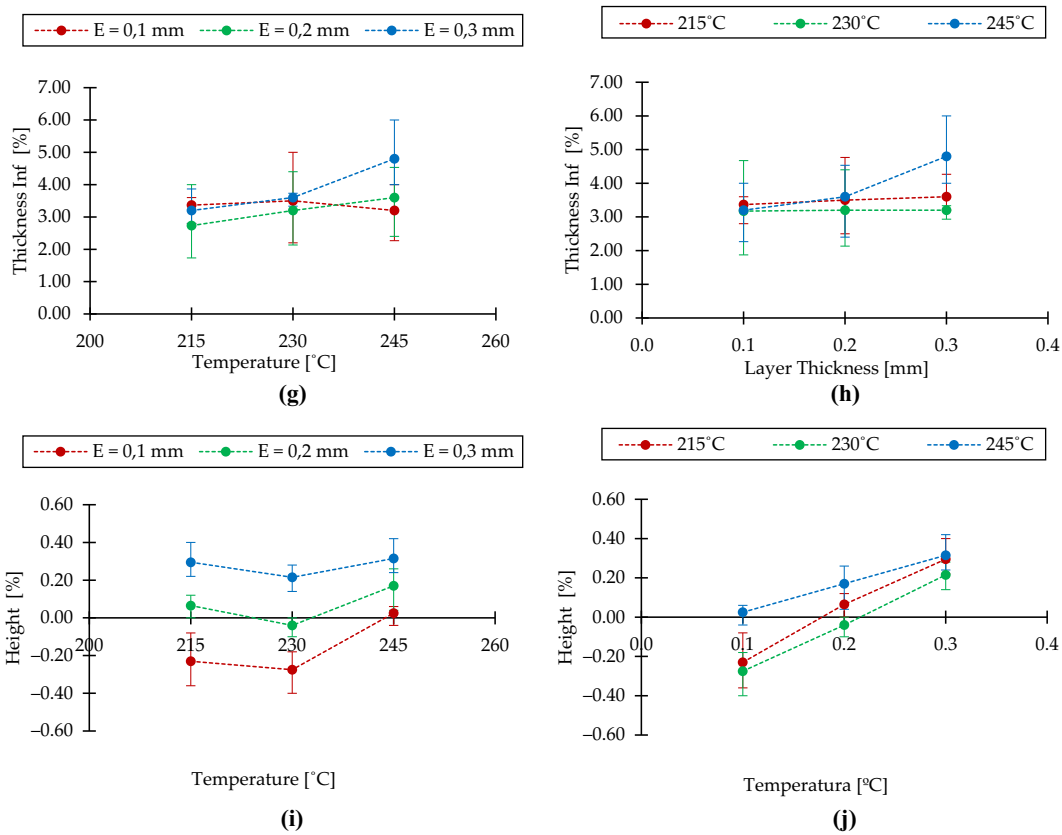

3.3 Macro and micro-geometrical analysis

For the RON deviation [Figure 10(a) and 10(b)], both the inner face and the outer face, the most significant parameter is the layer thickness [Figure 10(b)]. The fact that for the 0.1 mm thickness the dimensional deviations are less than for the 0.3 mm ones, with the 0.2 mm ones being the intermediate ones, can be because the lower the thickness, the less material is deposited in the layers and so, the layers cool faster while better maintaining their initial shape, having less time to deform due to the weight of the layers deposited on top of the printed ones.

There is also a clear difference between both faces, giving considerably lower values on the inside. The shape of the samples is different in the inside and outside. Concave (inside) and convex (outside). This can greatly influence on how the filament sits at the respective edges of the layer. Also, the fact that the outside diameter is larger than the inside affects the deviations as well. The printing temperature is not significant enough to present a results variation. This can be due to the CF reinforcement, that works against contraction, maintaining the material more stable. In Figure 6(b) and 6(c) can be appreciated the deposition starting point of each layer, how presents a greater deviation. This does not affect much the RON final value because it is treated as a mean value.

As for the CYN [Figure 10(c) and 10(d)], the evolution is similar as for RON. The lower the thickness, the less material is deposited in the layers, so the layers cool faster while better maintaining their initial shape. The printing temperature is also not significant, as can be appreciated in Figure 10(d).

For CON, as it can be seen in Figure 10(e) and 10(f), there is not a clear influence of the printing parameters because the results do not follow an obvious tendency. From Figure 10(e), it can be appreciated that for 0.1 mm, the lower the temperature the greater the deviations and 0.2 mm seems to have a more equilibrate tendency and 0.3 mm presents the inverse as for 0.1 mm. This can be explained because of contractions and shape deformation. For 0.1 mm, the material tends to cool faster and so, the higher the temperature the less contractions can occur because the material has more time to stabilize its temperature with the environment. As for 0.3 mm, this increase on the cooling time also gives more time to the material to deform plastically and so, the deviations are greater when the printing temperature are high. Figure 10(f) presents the same evolution. It can be seen that 0.1 and 0.3 mm have contrary evolutions. So, for CON, both the temperature and the layer thickness need to be taken into account, being 0.2 mm and 230°C the parameters that show more stabilize results.

As for COX [Figure 10(g) and 10(h)], a similar tendency as for CON can be appreciated, being 0.2 mm and 230°C the printing parameters that show steady results.

For the STR [Figure 10(i) and 10(j)], it can be seen that the deviation values on the inner and outer face are similar. This may be due to the manufacturing procedure: both the outer and inner faces are made in the same way, depositing the filament forming the circle of the outer or inner contour alike. Again, the printing temperature is not significant enough, which could be due to the CF reinforcement.

Finally, it is observed that the flatness values [Figure 10(k) and 10(l)] are more influenced, in this case, by the extrusion

Figure 10 Evolution of the geometrical parameters considered according to the temperature and the layer thickness, respectively: (a, b) oundness, (c. d) cylindricity, (e, f) concentricity, (g, h) coaxiality, (i, j) straightness and (k, l) flatness

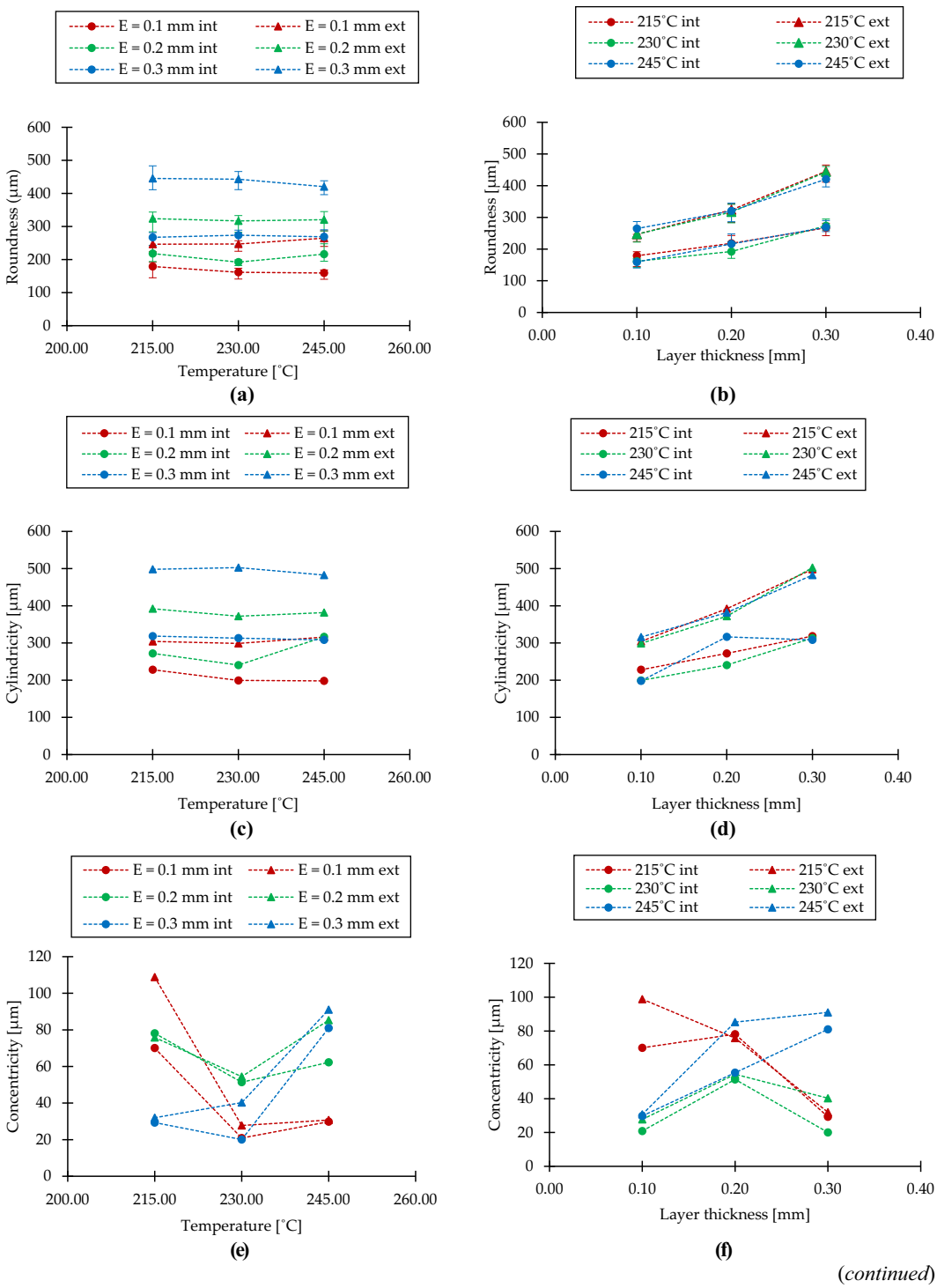

(*continued*)

Figure 10

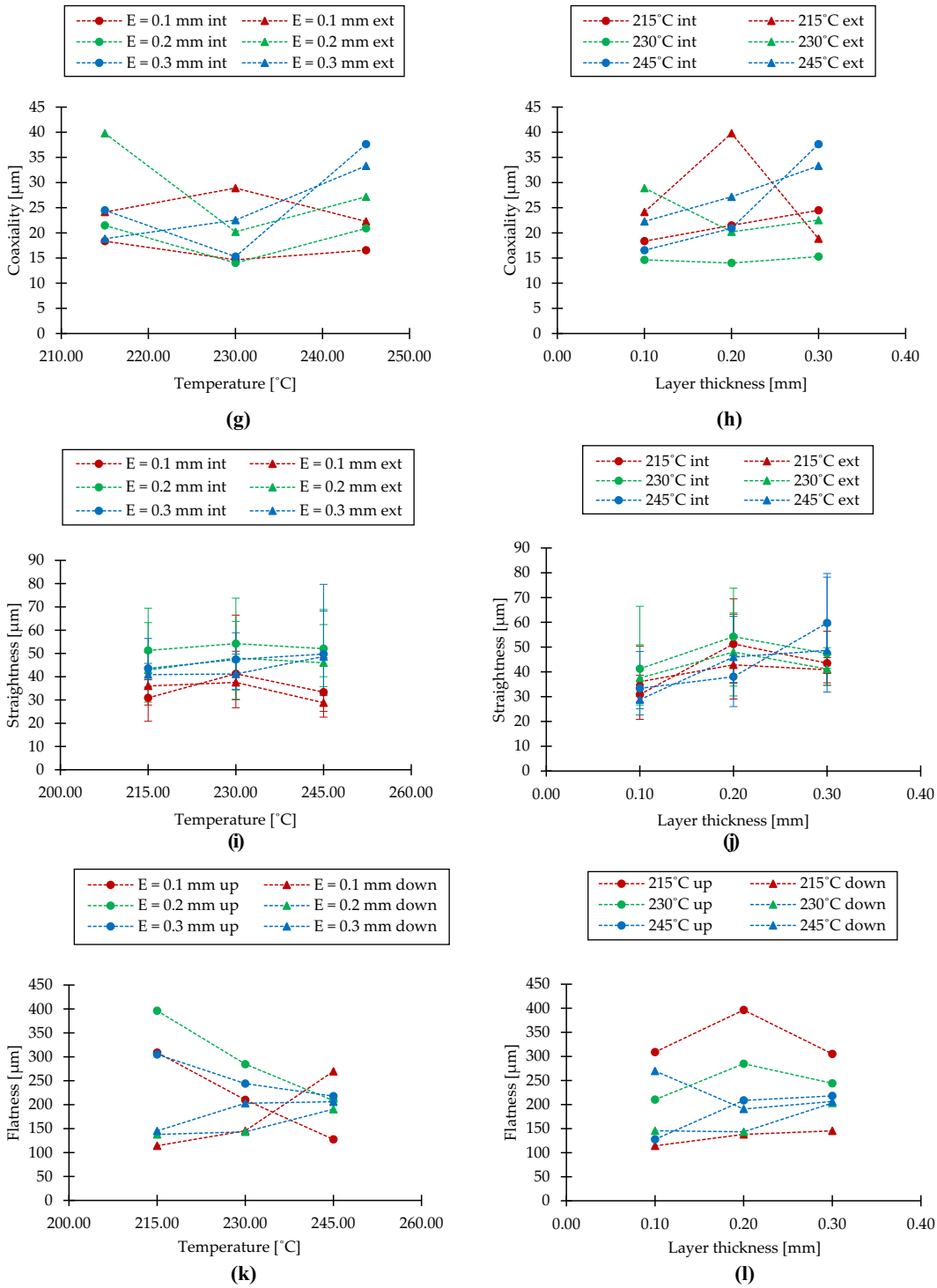

temperature. For the upper face, the largest deviation is for 215°C and the smallest for 245°C, while for the down face it is the other way around and tend to similar values as the upper one for the highest temperature. This difference may be because the lower face is supported by a raft, and its removal can affect the deviations. The higher the temperature, the higher the adhesion between layers is expected. So, when the raft is removed it causes more damage. On the contrary, the upper surface is free, it has no restrictions on movement of any kind, while the lower surface is restricted on both sides. In addition, the temperature of the print bed and the weight of the upper

Figure 11 Roughness results, exterior (a) and interior (b) Ra. Exterior (c) and interior (d) Rz (mm)

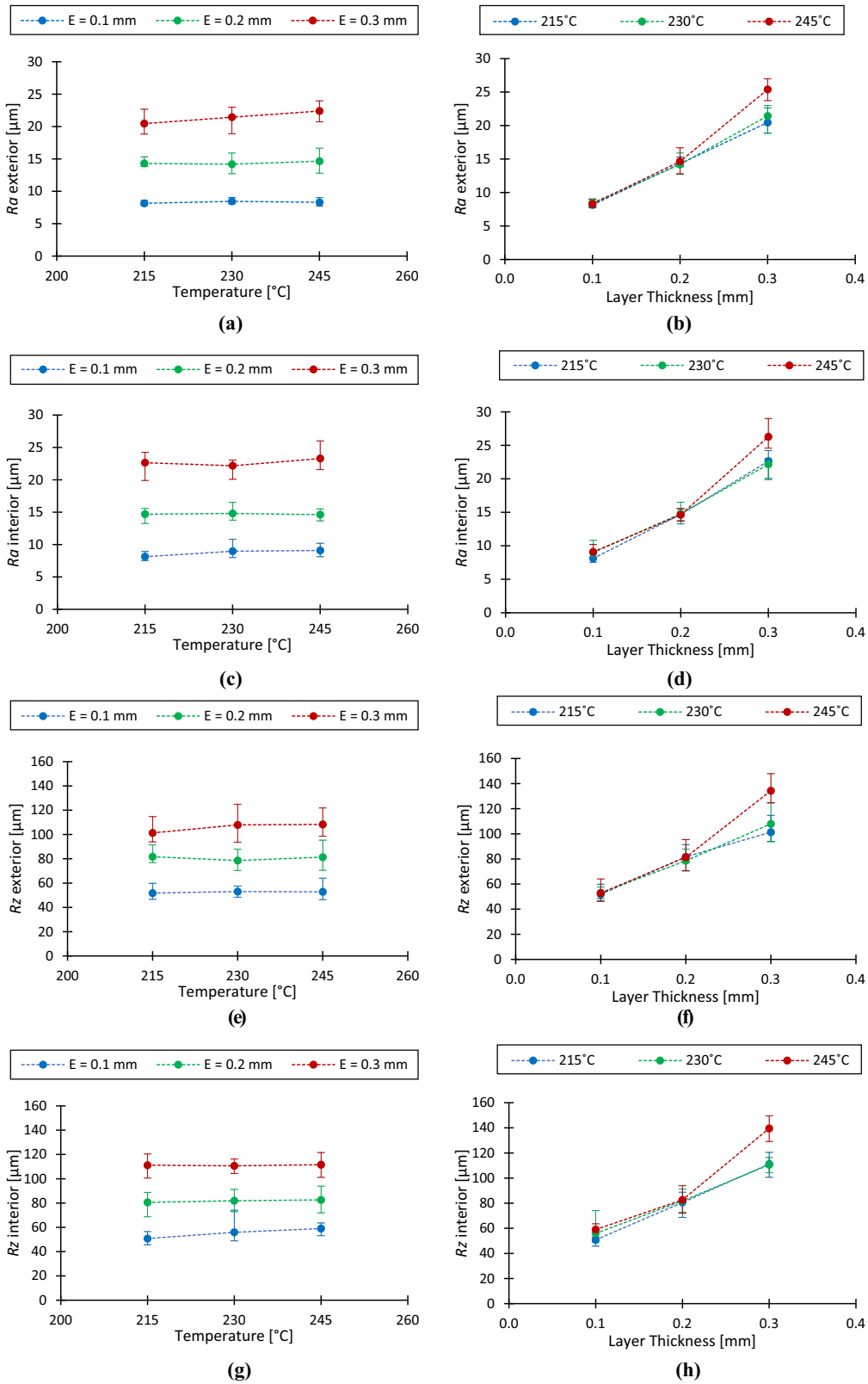

Table 3 Constants results for the parametric equation

GD	C	x	y	R^2
Dext	42.916	0.00429	0.00903	0.83
Dint	29.562	−0.00208	−0.00003	0.85
H	47.837	0.00388	0.00946	0.77
RON ext	714.28	0.48080	0.00765	0.92
RON int	2334.894	0.42792	−0.30812	0.90
CYL ext	1073.71	0.42490	−0.05503	0.94
CYL int	735.934	0.37558	−0.07247	0.78
SRT ext	43.864	0.24715	0.06346	0.36
SRT int	18.449	0.33553	0.26292	0.38
FLA sup	6.114×10^{13}	0.23618	−4.73068	0.74
FLA inf	1.151×10^{-07}	0.07377	3.90376	0.60
R_a ext	1.782	0.88981	0.65647	0.98
R_a int	1.932	0.89092	0.64981	0.97
R_z ext	4.267	0.69314	0.75272	0.95
R_z int	1.024	0.69110	1.02147	0.95

layers also affects the bottom surface. That is the way the tendency is not as much pronounced in that case. No significant trend is observed for layer thickness [Figure 10(l)].

As for the roughness (Figure 11), *Ra* increases its value as the layer thickness increases [Figure 11(a)], being the influence of temperature less significative [Figure 11(b)]. These results are consistent because the greater the thickness, the greater the thickness of the grooves that are formed due to the overlapping of the layers. Manufacturing the part vertically allows the roughness to be measured in the direction perpendicular to the layers. There is no significant difference between the values of the inner and outer face [Figure 11(c) and 11(d)].

Like *Ra*, *Rz* increases its value as the layer thickness increases [Figure 11(e)], with the influence of temperature being less significative [Figure 11(f)]. These results are also consistent because the greater the thickness, the greater the height of the grooves that are formed due to the superimposition of the layers. There is also no significant difference between the values of the inner and outer face [Figure 11(g) and 11(h)].

As it is shown, the roughness has a direct relation with the layer height. The thicker the layer, the higher the roughness.

3.4 Parametric model for macro-geometrical deviations

A parametric model (GD) can be adjusted for the experimental results obtained. This model relates some of the analyzed geometrical deviations with the printing parameters. This can be useful to predict these deviations before printing and adapt the printing parameter to obtain the geometry required. Different models were tested. The best fit was obtained for a potential model, as shown in equation (3).

$$GD = C \cdot E^x \cdot T^y \tag{3}$$

where C, x and y are constant. Table 3 shows the results obtained for these constants, for a reasonable determination coefficient R^2 = 0.75 – 0.99. The table shows the parameters for which the equation represents a good fit (Diameter, Height, RON, CYL, SRT, FLA, R_a, R_z).

Additionally, Figure 12 plots these parametric potential models in 3D, where each geometrical deviation is represented by a surface. As previously commented, it can be appreciated that the parameters studied show a strong dependence on the layer thickness over the temperature.

4. Conclusions

After analyzing all the results obtained, several conclusions can be drawn. For the printing speed considered, it can be seen that the results obtained, in general, are in good agreement with previous studies of different authors. So, it can be stablished that the speed can be increased and obtain good results and good printing parts. As for the dimensional control, the value of both the exterior and interior diameter is less than the nominal. However, the internal diameter is the one that presents the larger deviations due to the deposition mechanics of the filament. The layers are warm and compressed one to another, resulting in an oval shape. This decreases the internal radio and increases the external one. Also, the increment of the outer diameter compensates the shrinking of the material, having values closer to the nominal value.

The thickness value exceeds the nominal value in all cases because it is a function of the external and internal diameter and their difference. However, the lower part presents more deviation than the upper part due to the material cooling time. The down part in contact with the hot bed and is constantly receiving more warm material as the upper layers are being deposited. The push of the nozzle and the weight of the upper layers, coupled with the longer cooling time, results in more deformation than in the upper part.

For the height, a clear influence of the layer thickness is seen: the greater the thickness, the greater the value of the height. This can also be explained due to the oval deformation. The thinner the layer, the easier the deformation overcomes and so, the less height.

For the micro-geometric deviations, both *Ra* and *Rz*, there is a clear trend where the layer thickness clearly affects the results, and the temperature does not have a clear effect. The thicker the layer, the higher the roughness values due to the pics and valleys that are generated during the deposition of the layers.

As for the macro-geometric deviations, the most significant parameter has been the layer thickness. It has been observed that the greater the thickness, the greater the deviations for all the deviations analyzed. The outer face deviations are generally greater than on the inner face. This can be explained because of the convexity of the outer face, compared to the concavity of the inner face of the test piece. Also, for the temperature range studied, no clear trend is observed. This can be due to the material. Being PLA+CF, the CF works against contractions and maintains a more stable behavior.

Figure 12 Potential models for (a) exterior diameter, (b) interior diameter, (c) superior thickness, (d) inferior thickness, (e) height, (f) exterior Ra, (g) interior Ra, (h) exterior *Rz*, (i) interior *Rz*, (j) exterior RON, (k) interior RON, (l) exterior CYL, (m) interior CYL, (n) exterior SRT, (o) interior SRT, (p) superior FLA and (q) inferior FLA

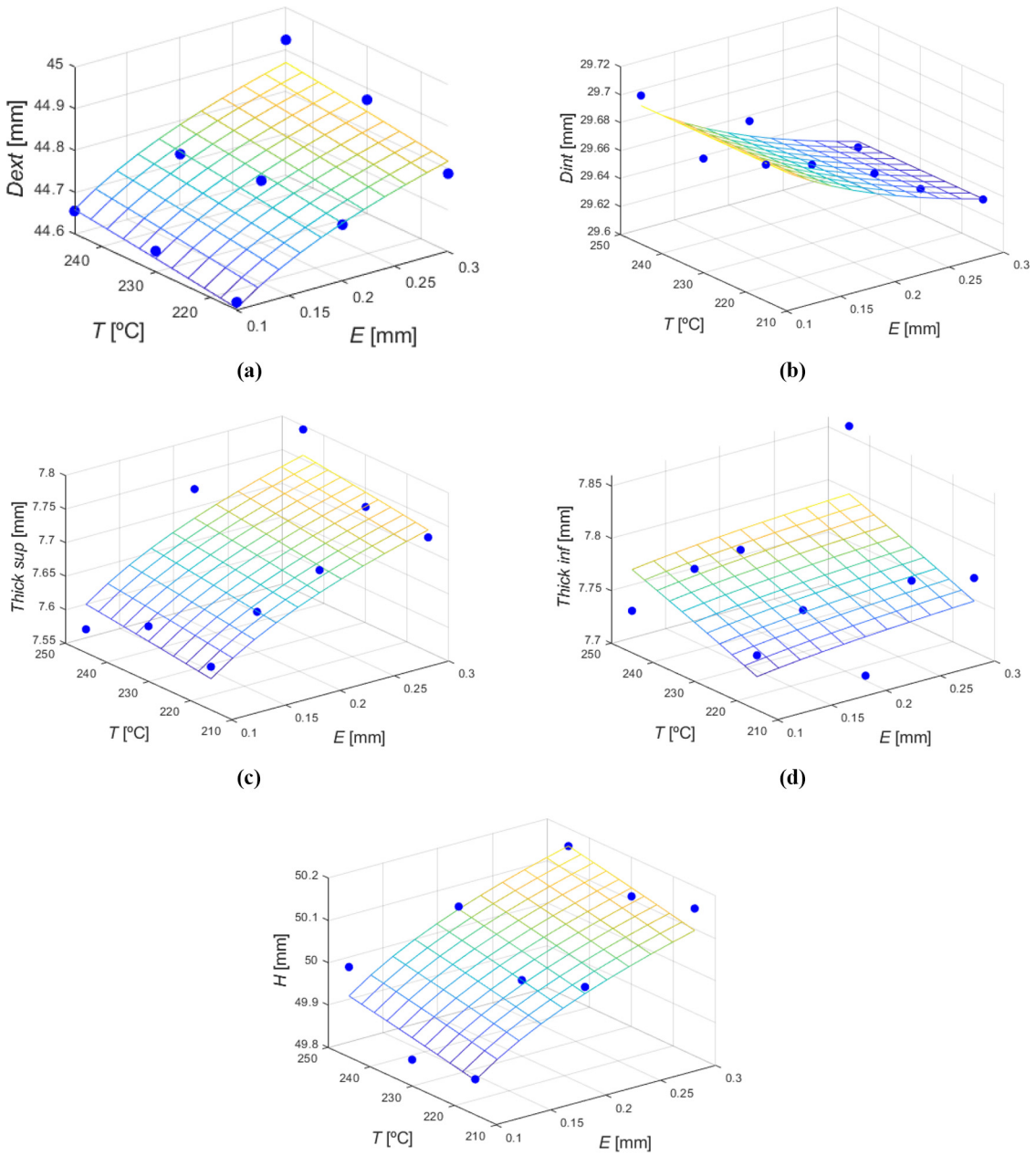

(*continued*)

For straightness, the values on the inner and outer face are similar, as the filament is deposited on both forming a circle. Likewise, for the different layer thicknesses and temperatures, no significant trend is found. As for the flatness, the most influential parameter is the extrusion temperature. For the upper face (free face) the greatest deviation occurs at 215°C and the least for 245°C, which can be explained due to the thermal shock and less time to cool down, because of the lower temperature difference with the environment. While for the down face (close to the hot bed), it is the other way around. This it is conditioned by three factors: the hot bed, the weight of the upper layers and the raft, which restrict the lower face.

For the layer orientation, all the measurements present higher deviations for the horizontal. The external diameter is even greater than its nominal value. The height is similarly affected, causing it to increase. Also, the macro-geometric deviations, are significantly higher than in the vertical ones, since, due to gravity and the plasticity of the still-hot filament,

Figure 12

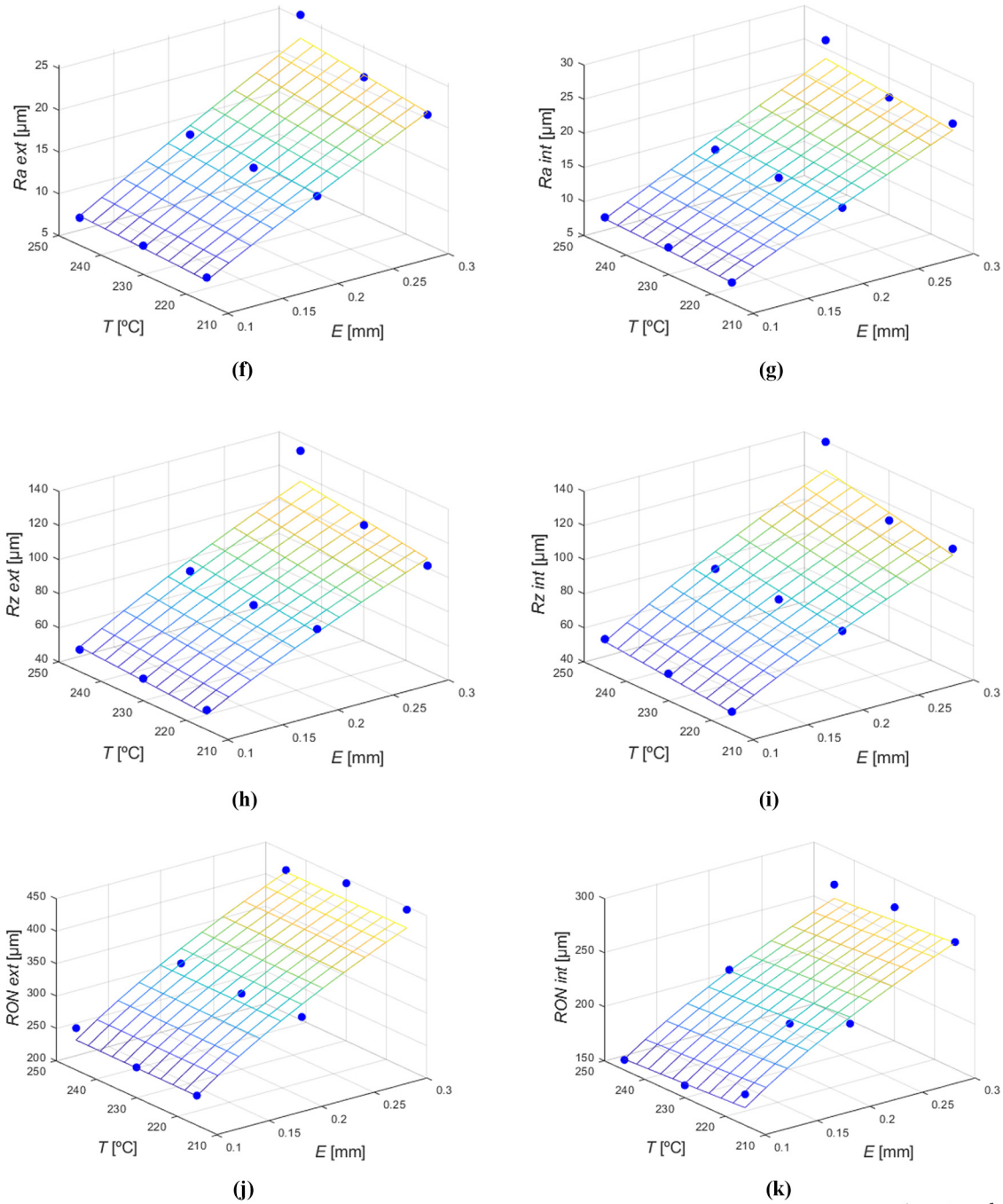

(*continued*)

the horizontal specimens find it more difficult to maintain their shape. A considerable part of the samples is either at a critical angle, which makes the filament tend to fall out, or without enough filling to have a consistent shape, due to the hollow interior.

Also, a set of potential parametric models were proposed for the macro and micro-deviations analyzed. These models exhibited a reasonable fitting in general, being R^2 = 0.7–0.9. These models may be useful to analyze the influence of the printing conditions (e, T) in these deviations before printing. It is necessary to point out that these models are useful in the range of variables evaluated and can be considered as a first step to obtain more complex models.

Finally, indicate that, among the parameters studied in this case study, the most decisive for the surface and geometric quality of the parts is the thickness of the layer and the printing orientation, observing in most cases that to obtain better results, it is best to reduce the thickness and choose vertical printing. However, the conclusions are drawn from the parameters considered and studied in this paper. Other printing

Figure 12

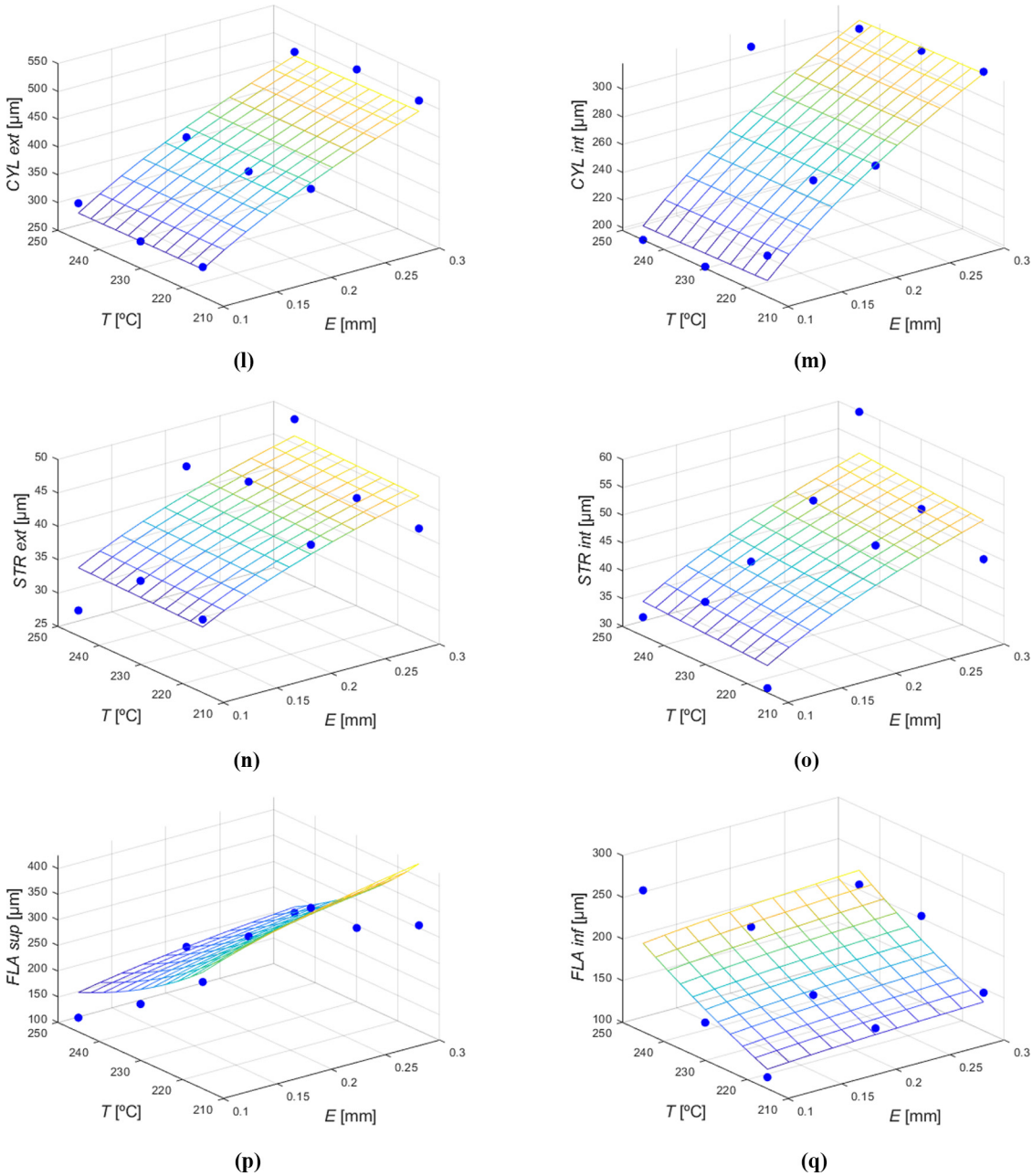

parameters and geometry options could and should be taken into account in future studies to increase the results data base and work with a complete optimization of the printing process.

References

Ahmed, A.A. and Susmel, L. (2017), "Additively manufactured PLA under static loading: strength/cracking behaviour vs deposition angle", *Procedia Structural Integrity*, Vol. 3, pp. 498-507, doi: 10.1016/J.PROSTR.2017.04.060.

Alam, F., Varadarajan, K.M. and Kumar, S. (2020), "3D printed polylactic acid nanocomposite scaffolds for tissue engineering applications", *Polymer Testing*, Vol. 81, p. 106203, doi: 10.1016/j.polymertesting.2019.106203.

Allison, A., Davis, M.A., Licht, F., Jaya Christiyan, K.G., Chandrasekhar, U. and Venkateswarlu, K. (2016), "A study on the influence of process parameters on the mechanical properties of 3D printed ABS composite", *IOP Conference Series: Materials Science and Engineering*, Vol. 114 No. 1, p. 12109, doi: 10.1088/1757-899X/114/1/012109.

Arbeiter, F., Spoerk, M., Wiener, J., Gosch, A. and Pinter, G. (2018), "Fracture mechanical characterization and lifetime estimation of near-homogeneous components produced by fused filament fabrication", *Polymer*

Testing, Vol. 66, pp. 105-113, doi: 10.1016/j.polymertesting.2018.01.002.

Arunkumar, N., Sathishkumar , N., Sanmugapriya , S.S. and Selvam , R. (2021), "Study on PLA and PA thermoplastic polymers reinforced with carbon additives by 3D printing process", *Materials Today: Proceedings*, Vol. 46, pp. 8871-8879, doi: 10.1016/J.MATPR.2021.05.041.

Bedi, P., Singh, R. and Ahuja, I.S. (2020), "'A comprehensive study for 3D printing of rapid tooling from reinforced waste 'thermoplastics", *Encyclopedia of Renewable and Sustainable Materials*, Elsevier, Amsterdam, pp. 114-144, doi: 10.1016/B978-0-12-803581-8.11495-X.

Bhagia, S., Bornani, K., Agrawal, R., Satlewal, A., Ďurkovič, J., Lagaňa, R., Bhagia, M., Yoo, C.G., Zhao, X., Kunc, V., Pu, Y., Ozcan, S. and Ragauskas, A.J. (2021), "Critical review of FDM 3D printing of PLA biocomposites filled with biomass resources, characterization, biodegradability, upcycling and opportunities for biorefineries", *Applied Materials Today*, Vol. 24, p. 101078, doi: 10.1016/J.APMT.2021.101078.

Bilkar, D., Keshavamurthy, R. and Tambrallimath, V. (2021), "Influence of carbon nanofiber reinforcement on mechanical properties of polymer composites developed by FDM", *Materials Today: Proceedings*, Vol. 46, pp. 4559-4562, doi: 10.1016/J.MATPR.2020.09.707.

Boğa, C. (2021), "Investigation of mechanical and fracture behavior of pure and carbon fiber reinforced ABS samples processed by fused filament fabrication process", *Rapid Prototyping Journal*, Vol. 27 No. 6, pp. 1220-1229, doi: 10.1108/RPJ-11-2020-0296.

Boğa, C. and Seyedzavvar, M. (2021), "A study on the effects of the interior architecture on the fracture toughness of 3D printed PLA samples", *European Journal of Science and Technology*, Vol. 32 No. 32, pp. 14-19, doi: 10.31590/EJOSAT.1039951.

Chacón, J.M., Caminero, M.A., García-Plaza, E. and Núñez, P.J. (2017), "Additive manufacturing of PLA structures using fused deposition modelling: effect of process parameters on mechanical properties and their optimal selection", *Materials & Design*, Vol. 124, pp. 143-157, doi: 10.1016/j.matdes.2017.03.065.

Culmone, C., Smit, G. and Breedveld, P. (2019), "Additive manufacturing of medical instruments: a state-of-the-art review", *Additive Manufacturing*, Vol. 27, pp. 461-473, doi: 10.1016/j.addma.2019.03.015.

Ding, S., Zou, B., Wang, P. and Ding, H. (2019), "Effects of nozzle temperature and building orientation on mechanical properties and microstructure of PEEK and PEI printed by 3D-FDM", *Polymer Testing*, Vol. 78, p. 105948, doi: 10.1016/J.POLYMERTESTING.2019.105948.

Dizon, J.R.C., Espera, A.H., Chen, Q. and Advincula, R.C. (2018), "Mechanical characterization of 3D-printed polymers", *Additive Manufacturing*, Vol. 20, pp. 44-67, doi: 10.1016/J.ADDMA.2017.12.002.

Doshi, M., Mahale, A., Singh, S.K. and Deshmukh, S. (2022), "Printing parameters and materials affecting mechanical properties of FDM-3D printed parts: perspective and prospects", *Materials Today: Proceedings*, Vol. 50, pp. 2269-2275, doi: 10.1016/J.MATPR.2021.10.003.

Durga Prasada Rao, V., Rajiv, P. and Navya Geethika, V. (2019), "Effect of fused deposition modelling (FDM) process parameters on tensile strength of carbon fibre PLA", *Materials Today: Proceedings*, Vol. 18, pp. 2012-2018, doi: 10.1016/J.MATPR.2019.06.009.

Ferreira, R.T.L., Amatte, I.C., Dutra, T.A. and Bürger, D. (2017), "Experimental characterization and micrography of 3D printed PLA and PLA reinforced with short carbon fibers", *Composites Part B: Engineering*, Vol. 124, pp. 88-100, doi: 10.1016/J.COMPOSITESB.2017.05.013.

Goh, G.D., Yap, Y.L., Agarwala, S. and Yeong, W.Y. (2018), "Recent progress in additive manufacturing of fiber reinforced polymer composite", *Advanced Materials Technologies*, Vol. 4 No. 1, p. 1800271, doi: 10.1002/admt.201800271.

González-Henríquez, C.M., Sarabia-Vallejos, M.A. and Rodriguez-Hernandez, J. (2019), "Polymers for additive manufacturing and 4D-printing: materials, methodologies, and biomedical applications", *Progress in Polymer Science*, Vol. 94, pp. 57-116, doi: 10.1016/J.PROGPOLYMSCI.2019.03.001.

Hanon, M.M. and Zsidai, L. (2021), "Comprehending the role of process parameters and filament color on the structure and tribological performance of 3D printed PLA", *Journal of Materials Research and Technology*, Vol. 15, pp. 647-660, doi: 10.1016/j.jmrt.2021.08.061.

Hanon, M.M., Zsidai, L. and Ma, Q. (2021), "Accuracy investigation of 3D printed PLA with various process parameters and different colors", *Materials Today: Proceedings*, Vol. 42 No. 5, pp. 3089-3096, doi: 10.1016/j.matpr.2020.12.1246.

Khan, S., Joshi, K. and Deshmukh, S. (2022), "A comprehensive review on effect of printing parameters on mechanical properties of FDM printed parts", *Materials Today: Proceedings*, Vol. 50, pp. 2119-2127, doi: 10.1016/J.MATPR.2021.09.433.

Kovan, V., Altan, G. and Topal, E.S. (2017), "Effect of layer thickness and print orientation on strength of 3D printed and adhesively bonded single lap joints", *Journal of Mechanical Science and Technology*, Vol. 31 No. 5, pp. 2197-2201, doi: 10.1007/S12206-017-0415-7.

Liao, G., Li, Z., Cheng, Y., Xu, D., Zhu, D., Jiang, S., Guo, J., Chen, X., Xu, G. and Zhu, Y. (2018), "Properties of oriented carbon fiber/polyamide 12 composite parts fabricated by fused deposition modeling", *Materials & Design*, Vol. 139, pp. 283-292, doi: 10.1016/J.MATDES.2017.11.027.

Liu, Z., Lei, Q. and Xing, S. (2019), "Mechanical characteristics of wood, ceramic, metal and carbon fiber-based PLA composites fabricated by FDM", *Journal of Materials Research and Technology*, Vol. 8 No. 5, pp. 3741-3751, doi: 10.1016/J.JMRT.2019.06.034.

Lokesh, N., Praveena, B.A., Sudheer Reddy, J., Vasu, V.K. and Vijaykumar, S. (2021), "Evaluation on effect of printing process parameter through taguchi approach on mechanical properties of 3D printed PLA specimens using FDM at constant printing temperature", *Materials Today: Proceedings*, Vol. 52, pp. 1288-1293, doi: 10.1016/J.MATPR.2021.11.054.

Raut, S., Jatti, V.S., Khedkar, N.K. and Singh, T.P. (2014), "Investigation of the effect of built orientation on mechanical properties and total cost of FDM parts", *Procedia Materials*

Science, Vol. 6, pp. 1625-1630, doi: 10.1016/J.MSPRO.2014.07.146.

Redwood, B., Schöffer, F. and Garret, B. (2017), *The 3D Printing Handbook*, 3D Hubs, p. 304, available at: www.3dhubs.com/3d-printing-handbook/ (accessed 18 February 2022).

Sedighi, I., Ayatollahi, M.R., Bahrami, B., Pérez-Martínez, M.A. and Garcia-Granada, A.A. (2020), "Mechanical behavior of an additively manufactured poly-carbonate specimen: tensile, flexural and mode I fracture properties", *Rapid Prototyping Journal*, Vol. 26 No. 2, pp. 267-277, doi: 10.1108/RPJ-03-2019-0055.

Singh, N., Singh, R. and Ahuja, I.P.S. (2018), "Recycling of polymer waste with SiC/Al2O3 reinforcement for rapid tooling applications", *Materials Today Communications*, Vol. 15, pp. 124-127, doi: 10.1016/J.MTCOMM.2018.02.008.

Spoerk, M., Holzer, C. and Gonzalez-Gutierrez, J. (2020), "Material extrusion-based additive manufacturing of polypropylene: a review on how to improve dimensional inaccuracy and warpage", *Journal of Applied Polymer Science*, Vol. 137 No. 12, p. 48545, doi: 10.1002/APP.48545.

Srinidhi, M.S., Soundararajan, R., Satishkumar, K.S. and Suresh, S. (2021), "Enhancing the FDM infill pattern outcomes of mechanical behavior for as-built and annealed PETG and CFPETG composites parts", *Materials Today: Proceedings*, Vol. 45, pp. 7208-7212, doi: 10.1016/J.MATPR.2021.02.417.

Sui, W. and Zhang, D. (2012), "Four methods for roundness evaluation", *Physics Procedia*, Vol. 24, pp. 2159-2164, doi: 10.1016/J.PHPRO.2012.02.317.

Suresha, B., Giraddi, V.V., Anand, A. and Somashekar, H.M. (2022), "Dynamic mechanical analysis of 3D printed carbon fiber reinforced polylactic acid composites", *Materials Today: Proceedings*, Vol. 59, pp. 794-799, doi: 10.1016/J.MATPR.2022.01.035.

Yang, C., Tian, X., Liu, T., Cao, Y. and Li, D. (2017), "3D printing for continuous fiber reinforced thermoplastic composites: mechanism and performance", *Rapid Prototyping Journal*, Vol. 23 No. 1, pp. 209-215, doi: 10.1108/RPJ-08-2015-0098.

Yao, S.S., Jin, F.L., Rhee, K.Y., Hui, D. and Park, S.J. (2018), "Recent advances in carbon-fiber-reinforced thermoplastic composites: a review", *Composites Part B: Engineering*, Vol. 142, pp. 241-250, doi: 10.1016/J.COMPOSITESB.2017.12.007.

Zhou, X., Hsieh, S.J. and Ting, C.C. (2018), "Modelling and estimation of tensile behaviour of polylactic acid parts manufactured by fused deposition modelling using finite element analysis and knowledge-based library", *Virtual and Physical Prototyping*, Vol. 13 No. 3, pp. 177-190, doi: 10.1080/17452759.2018.1442681.

Corresponding author

Carolina Bermudo Gamboa can be contacted at: bgamboa@uma.es